AD-A169 176 MEASUREMENT OF STRESS DISTRIBUTIONS IN ADHESIVE BONDED JOINTS(U) DENVER UNIV COLO COLL OF ENGINEERING P K PREDECKI ET AL. 04 APR 86 ARO-18358.4-MS 1/1

UNCLASSIFIED DAAG29-81-K-0150 F/G 20/11 NL

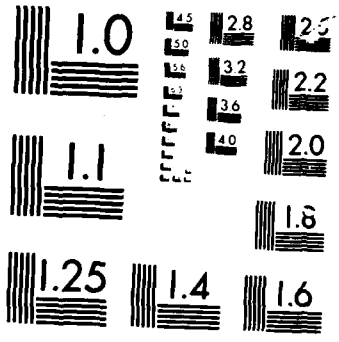

# MEASUREMENTS OF STRESS DISTRIBUTIONS IN ADHESIVE BONDED JOINTS

FINAL REPORT

Prepared by:

Paul K. Predecki, Charles S. Barrett and Alan B. Lankford
Engineering Dept., University of Denver, Denver, CO 80208

Submitted to:

U.S. Army Research Office
P.O. Box 12211, Research Triangle Park, NC 27709-2211

Contract
DAAG29-81-K-0150

APPROVED FOR PUBLIC RELEASE;
DISTRIBUTION UNLIMITED



The view, opinions, and/or findings contained in this report are those of the author(s) and should not be construed as an official Department of the Army position, policy, or decision, unless so designated by other documentation.

MASTER COPY - FOR REPRODUCTION PURPOSES

UNCLASSIFIED
SECURITY CLASSIFICATION OF THIS PAGE (When Data Entered)

| REPORT DOCUMENTATION PAGE | | READ INSTRUCTIONS BEFORE COMPLETING FORM |
|---|---|---|
| 1. REPORT NUMBER<br>ARO 18358.4-MS | 2. GOVT ACCESSION NO.<br>N/A | 3. RECIPIENT'S CATALOG NUMBER<br>N/A |
| 4. TITLE (and Subtitle)<br>MEASUREMENT OF STRESS DISTRIBUTIONS IN ADHESIVE BONDED JOINTS | | 5. TYPE OF REPORT & PERIOD COVERED<br>FINAL 08/17/81-02/28/86<br>6. PERFORMING ORG. REPORT NUMBER |
| 7. AUTHOR(s)<br>P. K. Predecki, C. S. Barrett, A. B. Lankford | | 8. CONTRACT OR GRANT NUMBER(s)<br>DAAG29-81-K-0150 |
| 9. PERFORMING ORGANIZATION NAME AND ADDRESS<br>University of Denver<br>Denver, CO 80208 | | 10. PROGRAM ELEMENT, PROJECT, TASK AREA & WORK UNIT NUMBERS |
| 11. CONTROLLING OFFICE NAME AND ADDRESS<br>U. S. Army Research Office<br>Post Office Box 12211<br>Research Triangle Park, NC 27709 | | 12. REPORT DATE<br>04/4/86<br>13. NUMBER OF PAGES |
| 14. MONITORING AGENCY NAME & ADDRESS(if different from Controlling Office) | | 15. SECURITY CLASS. (of this report)<br>Unclassified<br>15a. DECLASSIFICATION/DOWNGRADING SCHEDULE |

16. DISTRIBUTION STATEMENT (of this Report)

Approved for public release; distribution unlimited.

17. DISTRIBUTION STATEMENT (of the abstract entered in Block 20, if different from Report)

NA

18. SUPPLEMENTARY NOTES

The view, opinions, and/or findings contained in this report are those of the author(s) and should not be construed as an official Department of the Army position, policy, or decision, unless so designated by other documentation.

19. KEY WORDS (Continue on reverse side if necessary and identify by block number)

Adhesive bonds, X-ray diffraction, stress, peel stress, X-ray stress, curing stress, residual stress, acoustic emission, Al (6061), Al (5052), Be, single lap joint.

20. ABSTRACT (Continue on reverse side if necessary and identify by block number)

Triaxial stresses were determined by X-ray diffraction in the Al adherend of a single lap joint at an average depth of .033 mm from the Al/adhesive interface. Access to the joint was gained non-destructively by making one adherend of Be (relatively transparent to CuKα radiation) and the other of Al alloy (relatively opaque). The incident X-ray beam passed through the Be and the adhesive (FM-73M, American Cyanamid Co.) and was diffracted from the Al adherend adjacent to the Al/adhesive interface. Changes in the lattice spacing of the (511) + (333) reflection of Al compared with the stress free spacing were used to determine the

DD FORM 1 JAN 73 1473 EDITION OF 1 NOV 65 IS OBSOLETE

UNCLASSIFIED
SECURITY CLASSIFICATION OF THIS PAGE (When Data Entered)

strain and stress tensors along the bond. Measurements were made in the as-cured and loaded conditions, and on specimens containing an intentional debond.

Results for the loaded condition were compared with Texgap-2D finite element calculations for a nominally identical specimen at a depth .033 mm into the Al adherend. The comparison showed a general agreement in trends and magnitudes for all the stress components except at the extremities of the bond. In particular, the measured peel stress at one extremity was substantially larger than the calculated peel stress. The discrepancies between measured and calculated stresses can be explained qualitatively by the presence of an unintentional debond of depth < 0.5 mm at the one extremity.

Debonds of depth ≥ the X-ray beam width used are detected as abrupt slope changes at the edge of the debond, in all the applied stress distributions. These slope changes were also evident in the curing stress distributions.

In parallel experiments, acoustic emission measurements were made on contaminated and uncontaminated single lap joints similar to those used for the X-ray work. An approximate inverse relationship was found between the cumulative RMS counts to any applied load and the failure load of the specimen.

## A. STATEMENT OF PROBLEM STUDIED

At the present time there is considerable interest in the use of adhesive bonded joints for a variety of structural applications. The design of such joints is based mostly on finite element calculations and failure tests rather than on strain or stress measurements. To our knowledge, no measurements--other than those resulting from this study--have been made of stresses at or near the adhesive/adherend interface (where many bond failures occur). The difficulty of access to the interface and the presence of substantial gradients in these stresses make conventional methods inapplicable. There is also interest in developing NDE methods for detecting contaminated bonds of inferior strength.

The approach taken in this study was to gain access to the interface non-destructively by using X-rays. One of the adherends in a single lap joint was made relatively transparent to X-rays and the other relatively opaque. Incident X-rays from an X-ray tube then penetrated the first adherend (Be) and the adhesive (FM-73M*) and were diffracted from grains in the second adherend (Al, 6061 or 5052) adjacent to the adhesive/adherend interface. Changes in the lattice spacing of the (511) + (333) reflection of Al compared with the stress free spacing were used to determine the strain and stress tensors along the bond. Measurements were made in the as-cured and loaded conditions and on specimens containing an intentional debond. Results for the loaded condition were compared with finite element calculations for a nominally identical specimen. Acoustic emission measurements were made on clean and contaminated single lap joints similar to those used for the X-ray work.

It was known at the outset that the stresses to be measured would be small ($< \sim 20$ ksi) and the diffracted intensities weak because of absorption in the first adherend and the adhesive. The joint design and materials used were therefore optimized for the X-ray measurements.

## B. SUMMARY OF THE MOST IMPORTANT RESULTS

The geometry and dimensions (with minor variations) of the specimens used in the study are shown in Fig. 1. Measurements were made along the centerline of the specimen in the 1 direction using an irradiated area 7 mm high, in 2 direction x 1.4 mm wide, in 1 direction (0.56 mm wide near bond extremities). Curing stresses are shown in Figs. 2 and 3. The net applied stresses due to a tensile load of 2669N (600 lbs) in the 1 direction are shown in Figs. 4 to 7 together with the stresses calculated for the same specimen using the Texgap-2D finite element code** assuming plane strain.

The effects of a small intentional debond (0.5 mm deep in 1 direction) on the net stresses due to a tensile load of 2669N (600 lbs) applied in the

*Rubber modified epoxy with polyester matte (American Cyanamid, Havre de Grace, MD).

** Performed by Dr. Danton Gutierrez-Lemini, United Technologies Corp., Sunnyvale, CA 94086, to whom we are indebted.

1 direction are shown in Figs. 8 and 9. Debonds were made by inserting a .025 mm thick teflon film during bond preparation. The curing stresses (no load applied) in the vicinity of a deeper debond ($\sim$ 2.5 mm in 1 direction) are shown in Figs. 10 and 11.

## CONCLUSIONS

### Curing Stresses

(1) The curing stresses, $\sigma^c_{11}$ and $\sigma^c_{22}$ (Fig. 2) are quite large, $\sim$ 7 and 9 ksi respectively, as would be expected from the dissimilar expansion coefficients of the Be and Al ($\alpha_{Be} = 11.6 \times 10^{-6}/°C$, $\alpha_{Al} = 23.6 \times 10^{-6}/°C$). They decrease towards the ends A and B, most likely because of edge effects ($\sigma^c_{11}$ must go to zero at each end of the bond). These effects are more pronounced for $\sigma^c_{11}$ since the bond is only 12.7 mm wide in the 1 direction vs 25.4 mm in the 2 direction.

(2) The curing shear stress, $\sigma^c_{23}$ is zero as expected from symmetry, while $\sigma^c_{13}$ goes from positive to negative across the bond. The latter is due to the edge effects of the thermal contraction of the Al.

### Applied Stresses

(1) Measured stresses agreed reasonably well with the finite element stresses (Figs. 4-7) except near the extremities of the bond. In particular, the measured peel stress, $\sigma_{33}$, was significantly larger than the calculated peel stress near the end of the Be adherend (end B of the bond). Initially it was thought that the discrepancies were due to the stress singularities present at the reentrant angles at the bond extremities. Accordingly the number of elements near the corner where the Be adherend ended was increased from 13 to 224. This increased $\sigma_{11}$, $\sigma_{22}$ and $\sigma_{33}$ by 7.5%, 9.9% and 27% respectively at the extreme edge of the bond, while $\sigma_{13}$ became more negative by 43%--insufficient to account for the discrepancy. The fine mesh stress values are in fact the ones plotted in Figs. 4-7 for the last 0.5 mm of the bond. Finite element calculations were also made right at the Al/adhesive interface and were virtually identical with those .033 mm below the interface.

(2) The discrepancy looks like a displacement error of $\sim$ 1 mm in the 1 direction in the $\sigma_{33}$ X-ray measurements; however, the beam width is .56 mm here, so the displacement error is probably < .28 mm. Another error arises because the stress distribution across the irradiated area increases more rapidly than linearly as end B is approached. This would tend to make the measured values larger than the calculated values but would not account for the whole discrepancy.

(3) The reversals in the measured values of $\sigma_{13}$ near the bond extremities (Fig. 7) suggest that some other effect is involved. Possibilities include (a) a small crack or debond in fact exists at the end B, which alters and moves the stress distributions to the left slightly, (b) the adhesive layer near end B may be thicker than assumed for the X-ray calculations due to rounding of the Be edge during etching, (c) the structure and elastic constants of the adhesive may be different near the bond extremities (more adhesive, less matte) than the bond interior,

(d) the finite element calculation underestimates the normal stresses near end B and $\sigma_{13}$ near both ends.

(4) The X-ray elastic constants for the aluminum (511) + (333) reflection used with CuK$\alpha_1$ radiation were determined to be: $S_1 = -5.15 \times 10^{-6}MPa^{-1}$, $\frac{1}{2}S_2 = 1.91 \times 10^{-5}MPa^{-1}$ for Al 6061-T4 and $S_1 = -4.68 \times 10^{-6}MPa^{-1}$, $\frac{1}{2}S_2 = 1.70 \times 10^{-5}MPa^{-1}$ for Al 5052-H32 (stress relieved).

Effect of Intentional Debonds

(1) The debond edge was detectable as an abrupt slope change in all the applied stress distributions (Figs. 8 and 9) even with $\sim$ 0.5 mm deep debond present, compared with a beam width of 0.56 mm. The debond depth should be $\geq$ the X-ray beam width to improve detectability.

(2) The edge of the debond is marked by measurably higher normal stresses, $\sigma_{11}$, $\sigma_{22}$, $\sigma_{33}$ than measured at the same place with the same load applied in the absence of the debond. (Compare Figs. 4, 5, 6 with Fig. 8).

(3) A debond, if present at B in Figs. 4-7, must be < 0.5 mm in depth or abrupt slope changes seen in Figs. 8 and 9 would be evident. In fact the beginnings of such a slope change appear to be evident in $\sigma_{13}$ at both bond extremities (Fig. 7). Such a slope change in $\sigma_{13}$ ahead of the debond is seen to be more pronounced in Fig. 9.

(4) The maximum value of $\sigma_{33}$ determined near the end B increases in the order: finite element model (43 MPa), specimen with no intentional debond (54 MPa), specimen with 0.5 mm debond (70 MPa). This would be expected if a debond < 0.5 mm deep was in fact present in the specimen with no intentional debond. A quantitative estimate of this debond depth is not possible because of the relatively large X-ray beam width used (.56 mm).
The debond does not explain why no discrepancy between measured and calculated values of $\sigma_{33}$ is seen near end A (Fig. 6) even though the slope change in $\sigma_{13}$ suggests there is one present there.

(5) Debonds deeper than the beam width used are readily detectable in the residual stress distributions as seen in Figs. 10 and 11. Again the slope change in $\sigma^c_{13}$ can be seen in front of the debond.

Experimental Methods

(1) Position sensitive detectors, used either with or without a primary beam monochromator, are ineffective with these specimens. The peak/background ratio is much smaller than with a conventional scintillation counter and diffracted beam monochromator. The latter is essential to cut out the strong Compton scattering from the Be and the H and C in the adhesive.

(2) To reduce the errors in the stress measurements, the grain size of the diffracting adherend should be as fine as possible, consistent with good resolution of the $\alpha_1$, $\alpha_2$ doublet of the reflection used for the stress measurements. Al alloy 5052 (solution strengthened, non-heatable type) with H32 temper further stress relieved 30 min at 220°C proved to be satisfactory. Rocking the specimens during exposure also reduces the errors.

(3) The diffracted intensities from these specimens using CuKα radiation and a conventional X-ray tube are weak. Determination of a single diffraction peak ($10^4$ counts above background, integrated intensity) takes 2-10 mins exposure depending on $\psi$ angle. Complete stress determination on a bonded specimen takes several days. A synchroton source would greatly reduce this time plus provide greater flexibility in the choice of adherend materials and thicknesses.

Acoustic Emission

(1) In view of the long times required for the X-ray measurements, it was not practical to make AE measurements concurrently as originally intended. Instead A.E. measurements were made on standard single lap joints, 1" wide x 1/2" overlap using 1/8" thick adherends made from 6061-T6 aluminum and FM-73M or EA9309 (Hysol epoxy) adhesive. Two contaminants (Alconox detergent and polydimethyl siloxane vacuum grease in hexane) were used in various concentrations to produce contaminated bonds.

(2) A weak diffuse peak appears in the RMS emission rate between 65 and 85% of the failure load in both contaminated and uncontaminated bonds. Elsewhere the average RMS rate is roughly stable except for the last 5% of the failure load where there is a 10 to 50 fold increase in this rate.

(3) There is an approximate inverse relationship between the failure load and the total RMS counts to failure: the larger the failure load the fewer the total RMS counts. A similar relation holds for the cumulative RMS counts to any smaller load, e.g. for an uncontamined bond with a failure load of 2500 lbs there were 215 counts accumulated to 500 lbs, versus 5855 counts to 500 lbs for a contamined bond with a failure load of 625 lbs. The results were in general agreement with those obtained with adhesive bonds by other investigators.[1,2,3]

References

1. R. Hill, "The Use of Acoustic Emission for Characterizing Adhesive Joint Failure," NDT International 10(2), 63-72 (1977).

2. A. A. Pollock, "Acoustic Emission from Solids Undergoing Deformation." Ph.D. Thesis, University of London (1970).

3. J. H. Williams, Jr. and D. M. Egan, "Acoustic Emission Spectral Analysis of Fiber Composite Failure Mechanisms." Mat. Eval., 43-47 (Jan. 1979).

C. LIST OF PUBLICATIONS

1. "X-ray Diffraction Evaluation of Adhesive Bonds and Stress Measurement with Diffracting Paint," Charles S. Barrett and Paul Predecki, Advances in X-ray Analysis Vol. 24, p. 231, Plenum Publ. Corp., 1981 (Preliminary work before grant awarded).
2. "Diffraction Methods for Measurement of Stresses at Adhesive/Adherend Interfaces of Lap Joints," C. S. Barrett and Paul Predecki, Presented at 1982 TMS-AIME meeting, abstract published in J. Metals, 34(8), p. 46, August, 1982.

3. "Stress Determination in an Adhesive Bonded Joint by X-ray Diffraction," Paul Predecki and Charles S. Barrett, Advances in X-ray Analysis, Vol. 27, p. 251, Plenum Publ. Corp., 1984.
4. "Stresses in an Adhesive Bond at an Adhesive/Adherend Interface under Load," Paul Predecki, Charles S. Barrett, Alan B. Lankford, and D. Gutierrez-Lemini, J. Adhesion, 1986 (in press).
5. "X-ray Stress Determination in a Single Lap Joint Containing a Debonded Region," A. Lankford, C. S. Barrett, and Paul Predecki, Advances in X-ray Analysis, Vol. 29, Plenum Publ. Corp., 1986 (in press).
6. "X-ray Stress Analysis of Adhesively Bonded Joints," A. Lankford, M. S. Thesis, Univ. of Denver, Physics Dept., April 1986.

## D. PARTICIPATING SCIENTIFIC PERSONNEL

P. K. Predecki, P.I., Engineering Dept., University of Denver
C. S. Barrett, Co-P.I., Engineering Dept., University of Denver
A. B. Lankford, M.S. Graduate Student, Physics. (M.S. degree expected to be completed in April 1986).

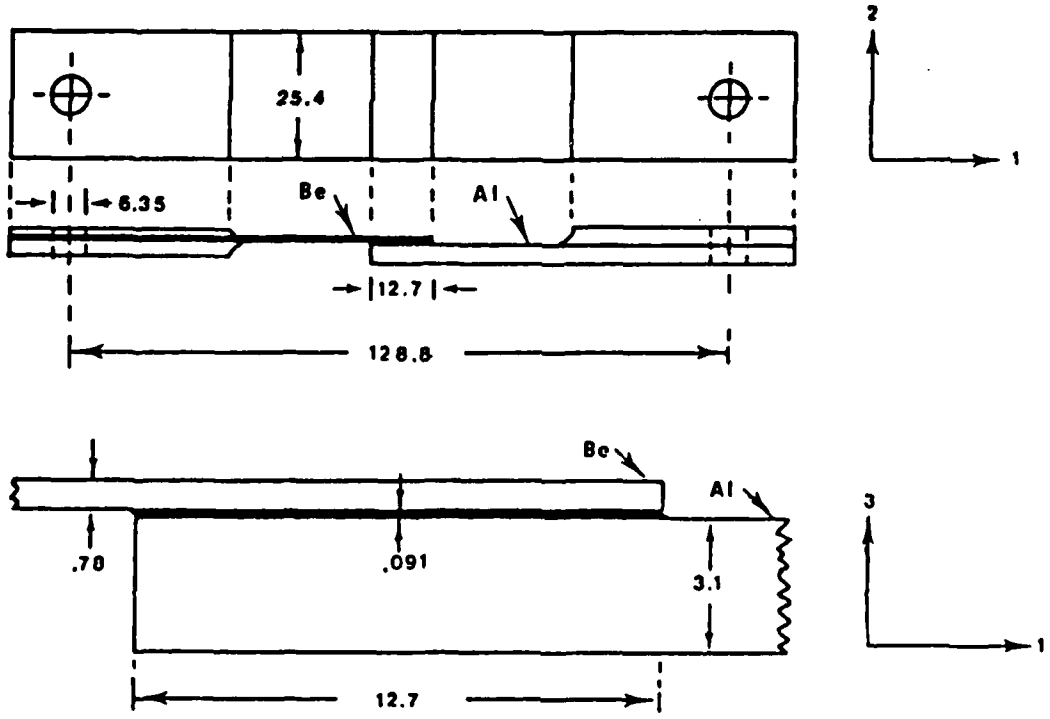


FIGURE 1 Dimensions in mm of the single lap joint specimen (ARO-23) used for stress determination. Tab thicknesses at the ends were made such that the central plane of the section at each clevis pin was coplanar with the plane of the adhesive layer at the center of the specimen.

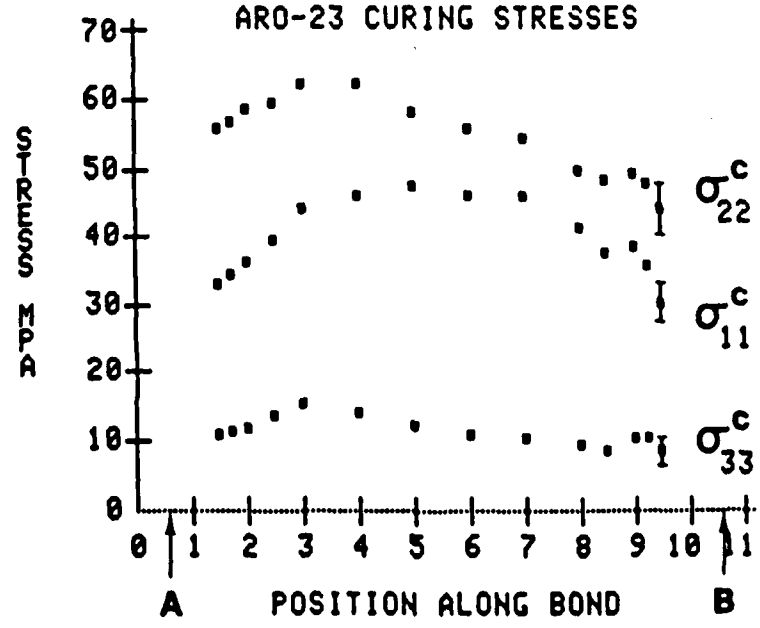


Fig. 2 . Curing normal stresses in the Al adherend at the adherend adhesive interface of the joint shown in Fig. 1. In this and subsequent figures, points A and B mark the ends of the Al and Be adherends respectively, stress measurements were made at 27.5°C (curing temperature was 125°C).

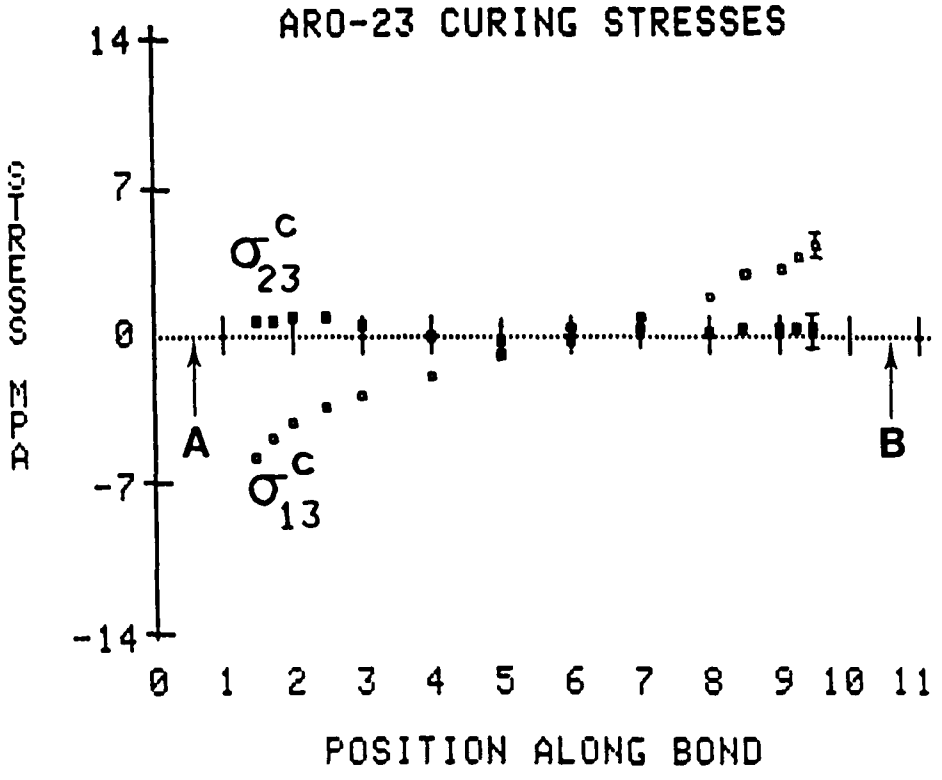


Figure 3. Curing shear stresses in the Al adherend at the adherend/adhesive interface of the joint shown in Figure 1.

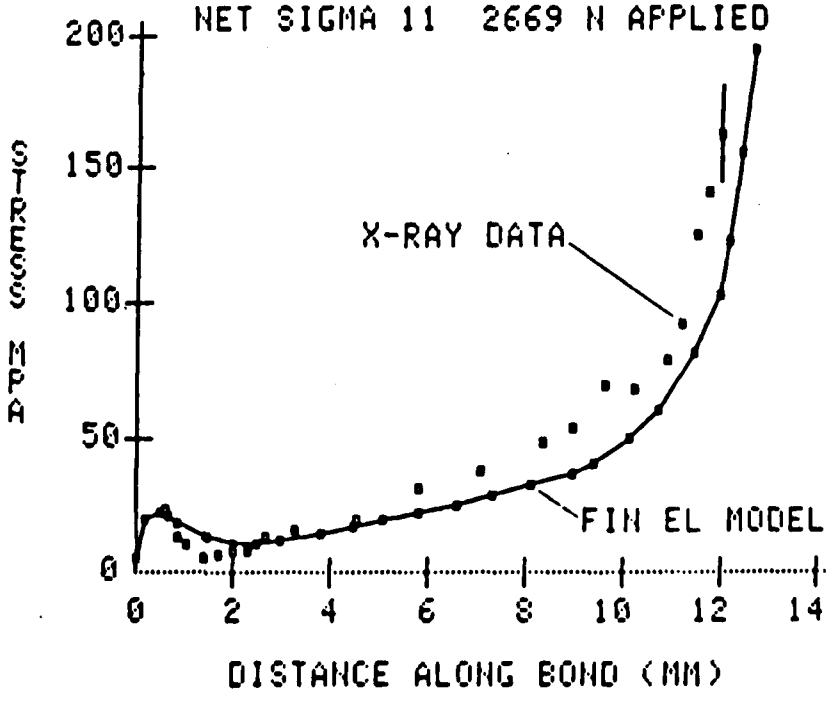


FIGURE 4 Comparison of normal stress, $\sigma_{11}$, measured by X-ray diffraction and calculated by the Texgap-2D finite element program (fin. el. model) along the Be/FM-73M/Al (6061-T4) single lap joint of Figure 1. Here and in Figures 5, 6 and 7 the measured and calculated stresses are in the Al adherend at a depth of 0.033 mm from the Al/adhesive interface; the edges of the Al and Be adhrends are at 0 and 12.7 mm, respectively.

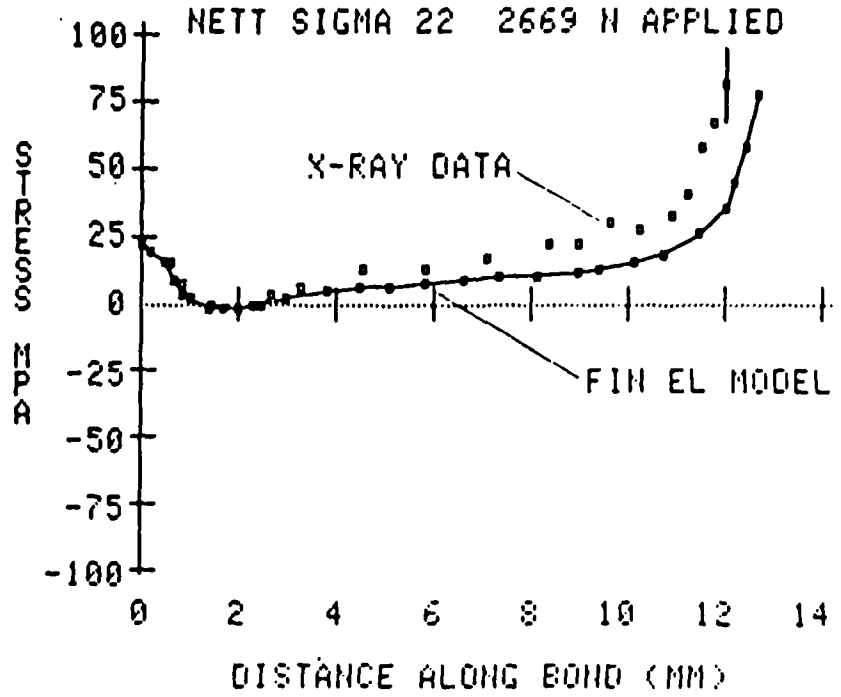


FIGURE 5 Comparison of normal stress $\sigma_{22}$ measured by X-ray diffraction and calculated by the Texgap-2D program along the Bc/FM-73M/Al (6061-T6) single lap joint of Figure 1.

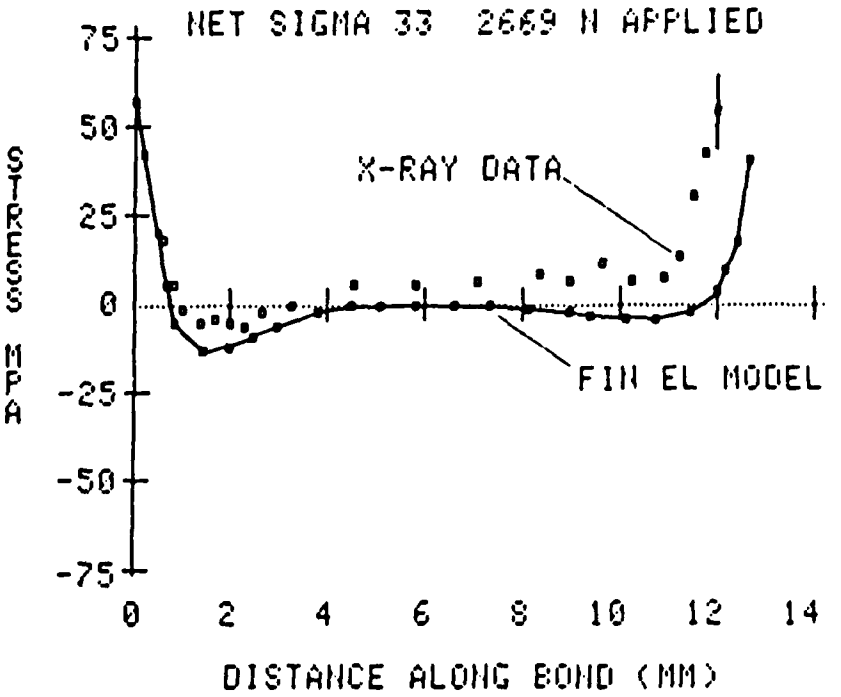


FIGURE 6 Comparison of normal peel stress $\sigma_{33}$ measured by X-ray diffraction and calculated by the Texgap-2D program along the Bc/FM-73M/Al (6061-T6) single lap joint of Figure 1.

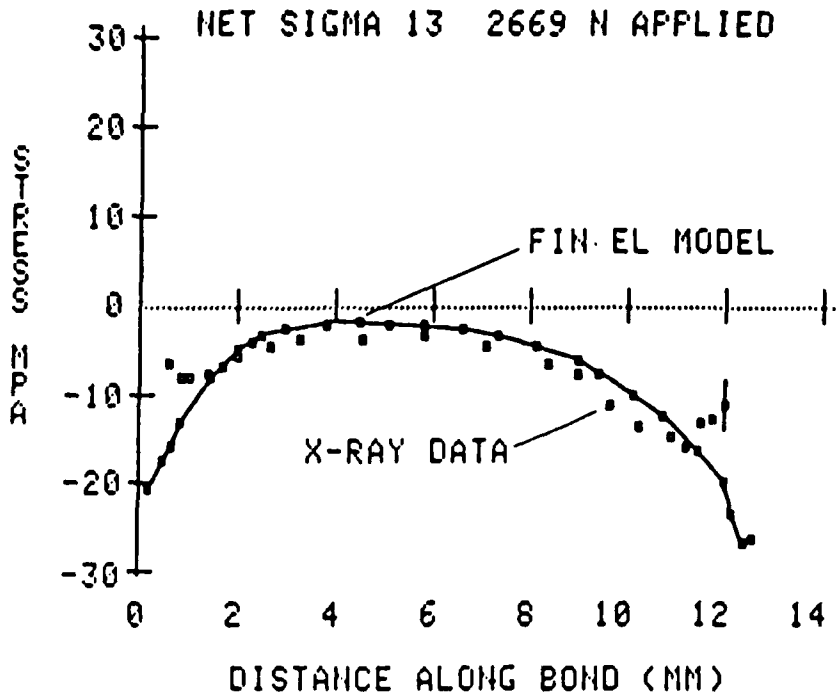


FIGURE 7. Comparison of shear stress $\sigma_{13}$ measured by X-ray diffraction and calculated by the Texgap-2D program along the Be/Fm-73M/Al (6061-T6) single lap joint of Figure 1.

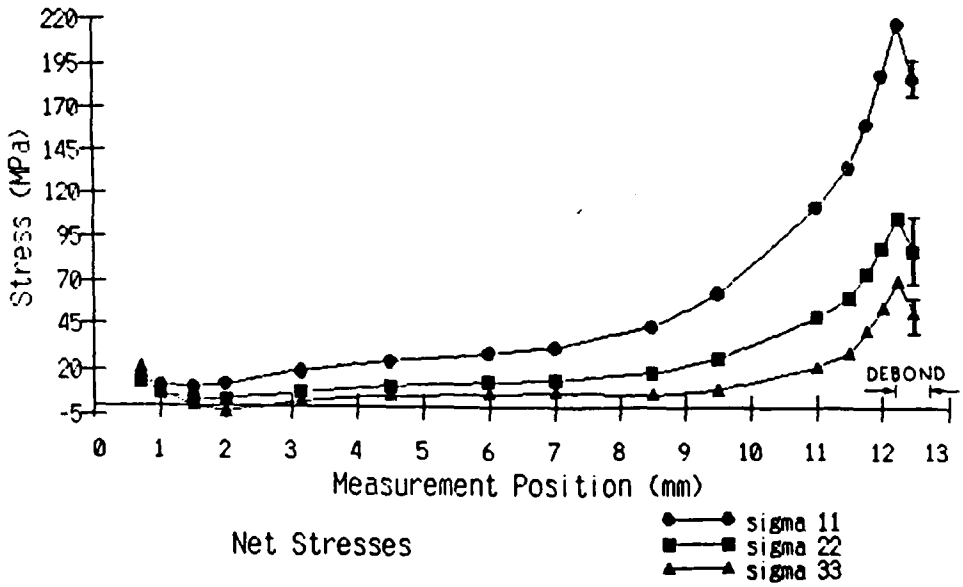


Figure 8. Net stresses $\sigma_{11}$, $\sigma_{22}$, and $\sigma_{33}$ due to an applied load of 2669N on specimen ARO-68 having the same dimensions as in Figure 1 except for a bond thickness of 0.069 mm and a debond 0.5 mm deep in the 1 direction at the end of the Be adherend. The Al adherend is alloy 5052 solution treated and stress relieved.

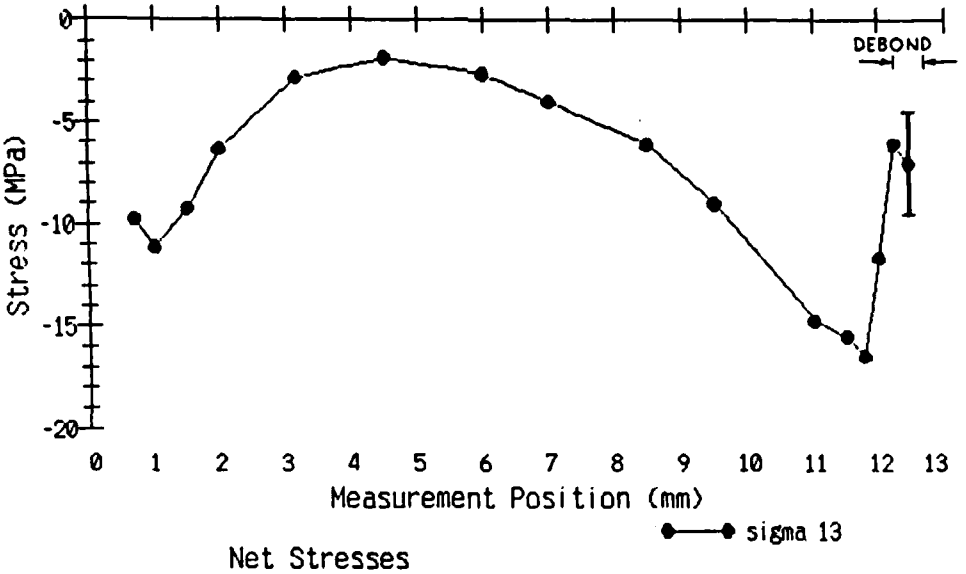


Figure 9. Net stress $\sigma_{13}$ for the same specimen and load as in Figure 8.

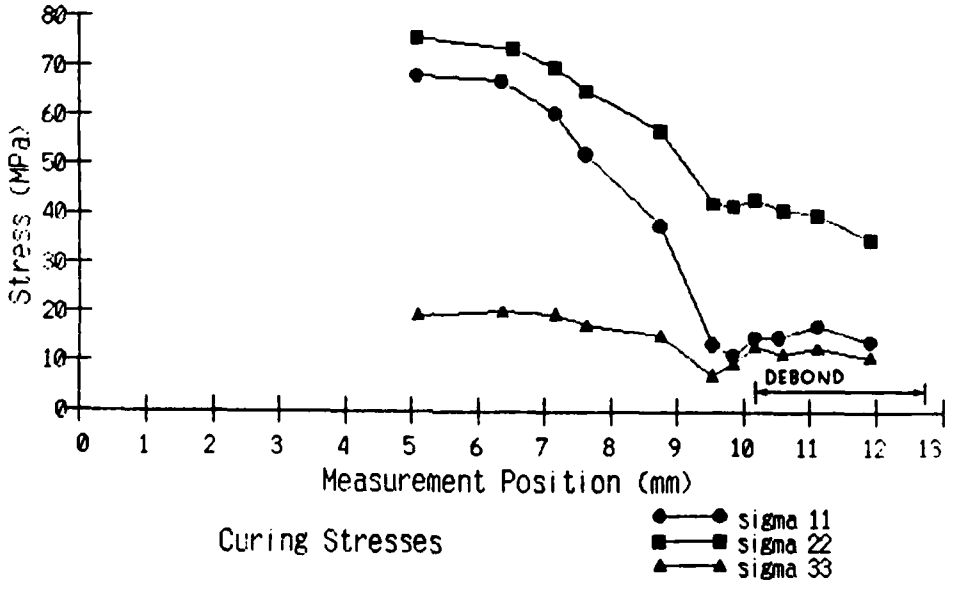


Figure 10. Curing stresses $\sigma_{11}^c$, $\sigma_{22}^c$, and $\sigma_{33}^c$ in the vicinity of the debond in a specimen (ARO-69) similar to that used in Figures 8 and 9, except that the debond depth in the 1 direction was 2.5 mm. Stress measurements were made at 25°C, curing temperature was 125°C.

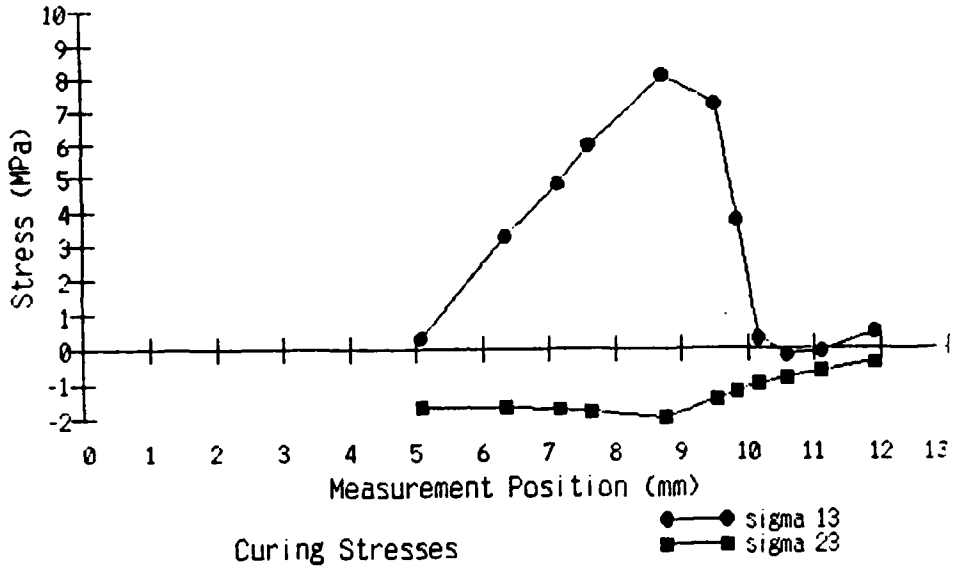


Figure 11. Curing stresses $\sigma^c_{13}$ and $\sigma^c_{23}$ for the same specimen and measurement conditions used in Figure 10.

END

DTIC

7-86